Colorimetry Technique for Scalable Characterization of Suspended Graphene

Cartamil Bueno, Santiago; Steeneken, Peter; Centeno, Alba; Zurutuza, Amaia; van der Zant, Herre; Houri, Samer

Important note
To cite this publication, please use the final published version (if applicable).
Please check the document version above.

Colorimetry technique for scalable characterization of suspended graphene

Santiago J. Cartamil-Bueno,[*,†] Peter G. Steeneken,[†] Alba Centeno,[‡] Amaia Zurutuza,[‡] Herre S. J. van der Zant,[†] and Samer Houri[*,†]

Kavli Institute of Nanoscience, Delft University of Technology, Lorentzweg 1, 2628CJ, Delft, The Netherlands, and Graphenea SA, 20018 Donostia-San Sebastián, Spain

E-mail: s.j.cartamilbueno@tudelft.nl; s.houri@tudelft.nl

Abstract

Previous statistical studies on the mechanical properties of chemical-vapor-deposited (CVD) suspended graphene membranes have been performed by means of measuring individual devices or with techniques that affect the material. Here, we present a colorimetry technique as a parallel, non-invasive, and affordable way of characterizing suspended graphene devices. We exploit Newton's rings interference patterns to study the deformation of a double-layer graphene drum 13.2 μm in diameter when a pressure step is applied. By studying the time evolution of the deformation, we find that filling the drum cavity with air is 2-5 times slower than when it is purged.

Keywords

Colorimetry, characterization technique, suspended, graphene, gas diffusion, pressure sensor

---

[*]To whom correspondence should be addressed
[†]Delft University of Technology
[‡]Graphenea

Introduction

Graphene, a monolayer of carbon atoms in honeycomb configuration, has become a subject of active study since its discovery in 2004.[1,2] Many potential applications that exploits its electromagnetic properties[3] and gas impermeability[4] have been proposed, from electronic switching[5] to water filtration[6] and pressure sensing.[7,8] Suspending graphene on circular cavities or trenches eliminates the negative impact of the substrate in its electrical conductivity,[9–12] which even allows the graphene to emit visible light,[13] and enables electro- or opto-mechanical actuation for mass, force and position sensing.[14?] However, graphene suspended movable devices are fragile and tend to break or collapse during the fabrication or measurement.[15,16]

Single-layer graphene (SLG) drums have been extensively studied, showing unique mechanical properties.[17–21] Many groups have demonstrated the scalability of CVD SLG drums and analyzed the statistical variation of their mechanical properties by measuring several drums with laser interferometry,[22,23] Raman spectroscopy,[15,24,25] and atomic force microscopy.[26,27] However, any attempt to commercialize graphene mechanical sensors is ineffective unless a characterization technique that is parallel, contactless, and affordable at the same time becomes available. Furthermore, CVD SLG usually contains gas permeable lattice defects and nanoscale pores due to its growth on imperfect substrates,[28] which blocks its application in gas pressure sensing devices that require impermeable membranes. A possible route to overcome this difficulty is to stack several CVD layers to reduce the probability of having nanopores from different layers aligned on the same spot.[29]

In this work, we introduce a new non-invasive optical technique to characterize the mechanical properties and the permeance of large arrays of suspended graphene membranes that is similar to Cornu's interference[30] and Fizeau interference[31] methods. We observe Newton's rings on a suspended CVD double-layer graphene (DLG) drumhead when applying a pressure difference between inside and outside of the cavity, which allows us to study the deformation of this mechanical system. We find that the rate of volume change is differ-

ent for purging and filling the cavity with air. Based on these observations, the permeance of the DLG membrane is determined and found to be two to three orders of magnitude higher than that of pristine graphene.

Device fabrication starts with a silicon substrate covered with 600 nm of thermally-grown SiO_2. Circular cavities of different diameters are patterned and etched through the oxide by means of reactive ion etching. Afterwards, a double-layer graphene, made by stacking two SLG CVD graphene layers, is transferred onto the SiO_2/Si substrate using a semi-dry transfer technique, thus resulting in suspended CVD-DLG drums. In this paper, we use DLG membranes because its absorption in the visible spectrum of light is at least twice that of SLG, which increases its reflectance while remaining highly transparent.[32]

Upon the application of a pressure difference between the inside of the cavity P_{int} and the outside of the cavity P_{ext}, the circular membrane is deformed. The drum deflects inward (upward) if the pressure difference $\Delta P = P_{ext} - P_{int}$ is positive (negative). Figure 1a shows an image of a DLG drum of 13.2 μm in diameter under white light illumination with $\Delta P \approx 1$ bar (top) and $\Delta P = 0$ (bottom). When the membrane is highly deflected as in Figure 1a, top panel, the circular geometry of the device causes the creation of concentric rings, which are also known as Newton's rings.[33] Progressively with time, air fills the cavity until P_{ext} and P_{int} become equal, resulting in a homogeneous color across the whole drum (Figure 1a, bottom panel).

When illuminated, part of the light is reflected from the suspended membrane I_g, and interferes with the light that crossed the membrane and is reflected from the bottom of the cavity I_s. This interference is constructive or destructive depending on the illumination wavelength and the distance separating the two surfaces. Since the absorption and internal reflections of the circular DLG membrane play a small role in the interference, the total reflected intensity for a given wavelength λ at a distance r from the center would be approximately $I(r) = I_g + I_s + 2\sqrt{I_g I_s} \cos\left(\frac{4\pi}{\lambda}\left(g_0 - \delta(r)\right) + \phi\right)$, where g_0 is the gap distance between the non-deflected membrane and the bottom of the cavity, $\delta(r)$ is the radial deflection, and
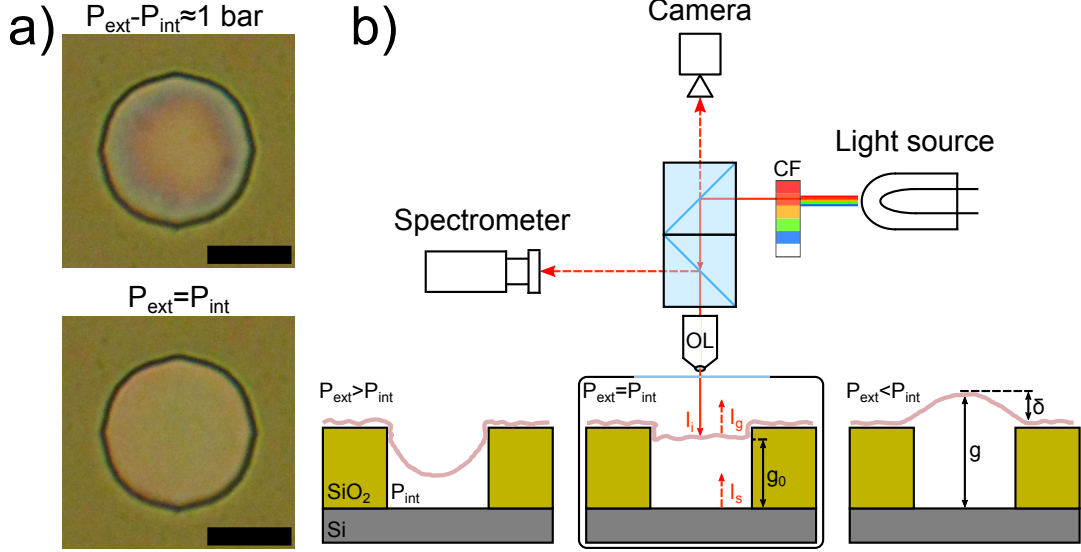
Figure 1: Newton's rings in a graphene drum and colorimetry setup. (a) Top: White light camera image of a downward deflected CVD double-layer graphene drum (13.2 μm in diameter) showing Newton's rings when the pressure difference between outside and inside the cavity is about 1 bar. Pressure-induced deflection of the drumhead changes the gap distance of the optical cavity radially. Bottom: After a certain time in an atmospheric environment, the cavity pressure is balanced and the drumhead is flat again, showing an homogeneous color. Scale bars are 10 μm. (b) Colorimetry setup: a customized optical microscope with a 100x objective lens (OL) and Köhler illumination is used for imaging the suspended graphene drum. White light from a Halogen lamp goes through a color filter (CF), and the intensity reflected from the drum I_g and the silicon substrate I_s is collected by a calibrated consumer camera and a spectrometer. Depending on the pressure difference, the drumhead bends downwards (left panel), remains flat (center panel) or bulges up (right panel).

ϕ is the phase change induced by the reflecting surfaces.[34]

To fully exploit this phenomenon for fast mechanical and permeance characterization of suspended membranes, we use monochromatic illumination. For this purpose, a cost-effective customized optical microscope setup with Köhler illumination using a simple white light Halogen lamp (Thorlabs OSL2) as an effective multi-wavelength source is built as shown in Figure 1b. A consumer camera (Canon EOS 700D) collects the total reflected intensity from each point of the drum that is placed inside a vacuum chamber. Monochrome RAW images are taken at a particular wavelength by using color filters (FWHM 4-10 nm). The intensity values from the CMOS camera are calibrated to correct for gamma compression[35]

(for more details, see Supporting Information). Furthermore, the reflectance is determined by applying $\mathcal{R} = \frac{I}{I_s}\mathcal{R}_s$, where $\mathcal{R}_s$ is the silicon reflectivity,[34] and I_s is the reflected intensity measured from an uncovered circular cavity. This normalization also cancels the inhomogeneous spectral intensity of the source and eliminates the impact of changes in the illumination intensity over time.

The radial deflection function of a circular membrane with radius R can be approximated by the maximum deflection at the center δ_c multiplied by the profile function $f(r) = 1 - 0.9\frac{r^2}{R^2} - 0.1\frac{r^5}{R^5}$.[36] Then, the reflectance as a function of r becomes

$$\mathcal{R}(r) \propto \cos\left(\frac{4\pi}{\lambda}\left(g_0 - \delta_c f(r)\right) + \phi\right) = \cos\left(\Omega f(r) + \phi'\right), \tag{1}$$

where $\Omega = -\frac{4\pi}{\lambda}\delta_c$ and $\phi' = \frac{4\pi}{\lambda}g_0 + \phi$ are the spatial frequency and phase of the Newton's rings. Therefore, $\mathcal{R}(r)$ depends on the wavelength and the maximum deflection. Figure 2a shows three monochromatic images of the drum for different wavelengths (λ=460 nm, 532 nm, and 660 nm) at $\Delta P \approx 1$ bar. Note that shorter wavelengths result in higher spatial frequency Ω. To improve the data analysis, especially for the short-wavelength noisy images, we take advantage of the centro-symmetry of the device and perform a radial average as shown in the figure for the corresponding monochromatic images. By fitting the radial-averaged reflectance to Eq. 1, it is possible to obtain a value of Ω and hence δ_c. In the case of the Newton's rings in Figure 2, the extracted center deflection is δ_c=-262 nm.

The Newton's rings fitting can be used to study the change in pressure-induced deflection with time, and therefore measure the permeance of the drum. The time-dependent maximum deflection as obtained for λ=532 nm illumination is shown in Figure 3 for both purging the air (top) and filling the cavity (bottom). We observe that the gas escapes from the cavity faster than when it has to fill it. As a technical remark, we also observe that the value of δ_c saturates around 70 nm due to the inaccuracy of fitting the data to Eq. 1 in the limit of small deflections. To understand these rate differences we model the gas filling and purging of the cavity using the ideal gas law, and Hooke's law considering only the non-linear term
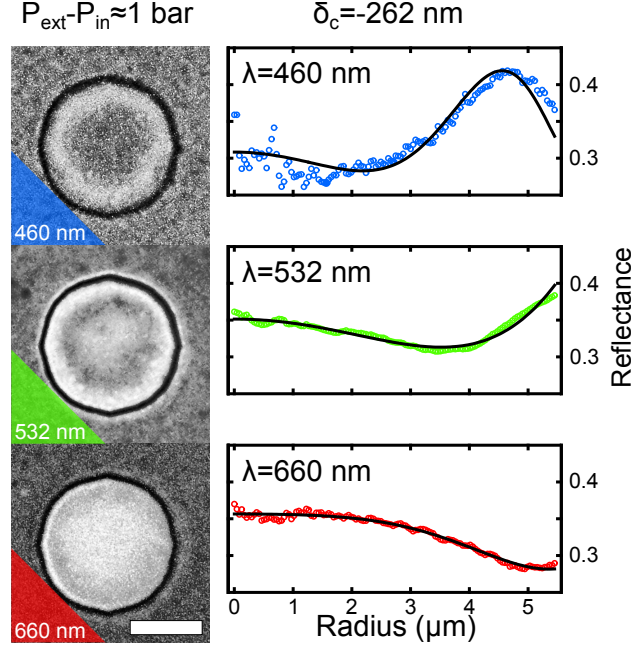
Figure 2: Radial reflectance profile across the drum. On the left, reflectance profile of the drum for different wavelengths at the same pressure difference as in Figure 1a (top). Scale bar is 10 μm. On the right, the radial-averaged reflectance (circles) of the corresponding wavelengths. The Newton's rings fit (line) gives a center deflection value of δ_c=-262 nm.

for large deflections.[37] The molecular flux from/to the inside of the cavity at large deflections is

$$\frac{\mathrm{d}n}{\mathrm{d}t} = \frac{4bk_3\delta^3 + 3g_0k_3\delta^2 + AbP_{ext}}{RT}\frac{\mathrm{d}\delta}{\mathrm{d}t}, \tag{2}$$

with positive deflection when purging and negative deflection when filling, and where R is the universal gas constant, T=300 K is the temperature, k_3 is the nonlinear spring constant of the drum and A, its area; b=0.52 is a geometric volume factor from the profile of a deflected circular membrane[38] (see Supporting Information). Equation 2 has two different solutions that depend on whether the drum is bulged upward or inward. Furthermore, the equation predicts that the molecular flux at large deflections depends on the external pressure: when the chamber is pumped ($P_{ext} \approx 0$), the gas escapes the drum cavity faster than when the chamber is vented ($P_{ext} \approx 1$ bar) and the cavity is slowly filled. This difference

in behavior between purging and filling of the cavity is corroborated in Figure 3 qualitatively, and discussed further in the Supporting Information.
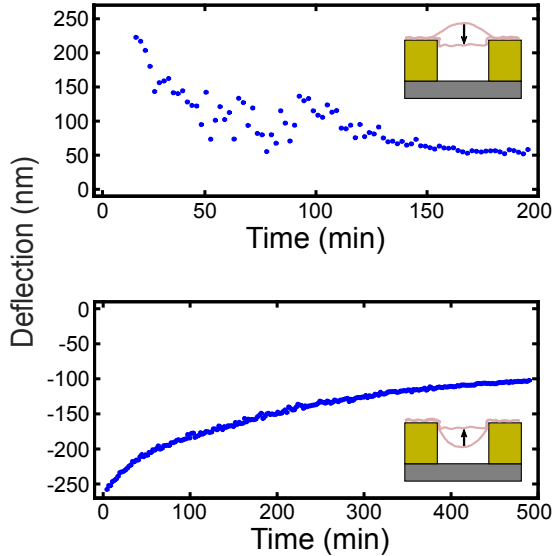

Figure 3: Time evolution of the deflection during purging and filling of the cavity. (a) The Newton's rings fitting is applied to a series of reflectance profiles of the same drum for λ=532 nm, resulting in the change of deflection while the drum returns to pressure balance (blue points). When the gas is escaping the cavity (top), the deflection returns to zero faster than in when the gas is filling the cavity (bottom). The Newton's rings fitting becomes inaccurate at small deflections.

To extract the permeance quantitatively, we consider the small deflection limit. In this linear-deflection regime, the cavity volume can be assumed to be constant and the mechanical response of the drum is governed by its linear stiffness. Under these conditions the membrane deflection is given by a simple decaying exponential $\delta(t) = \delta_\infty + \delta_0 e^{-t/\tau}$ for both purging and filling, where $\tau = \frac{A^2 g_0}{\mathcal{P}RT}$ is the time constant of the system, $\mathcal{P}$ is the permeance of the membrane,[39] and δ_∞, its position at rest which does not need to be zero due to side-wall adhesion.[15,40] In addition, for small deflections, the drum reflectance averaged over its area $\mathcal{R}_{drum}$ is directly proportional to the deflection, and can therefore be expressed as $\mathcal{R}_{drum}(t) = A + B\,e^{-t/\tau}$ (see Supporting Information for the derivation). The drum averaged reflectance is shown in Figure 4 for two wavelengths, 460 nm (blue circles) and 600 nm (orange circles), for both cavity filling and purging. As the large deformation regime subsides after 200 minutes

for the purging experiment and 1000 minutes for the filling experiment, the reflectance in the linear regime decays exponentially with time. This part of the curves is then fitted to obtain the time constant of the drum. The fitted time constants and the inferred permeance values are summarized in Table 1 for different wavelengths for the two experiments. It is worth noting that the drum's reflectance decays to different values in the case of the purging and the filling experiments as can be seen in Figure 4. The shift in the reflectance of the drum at rest could be an indication of the presence of side-wall adhesion or slack that changes the effective cavity depth.
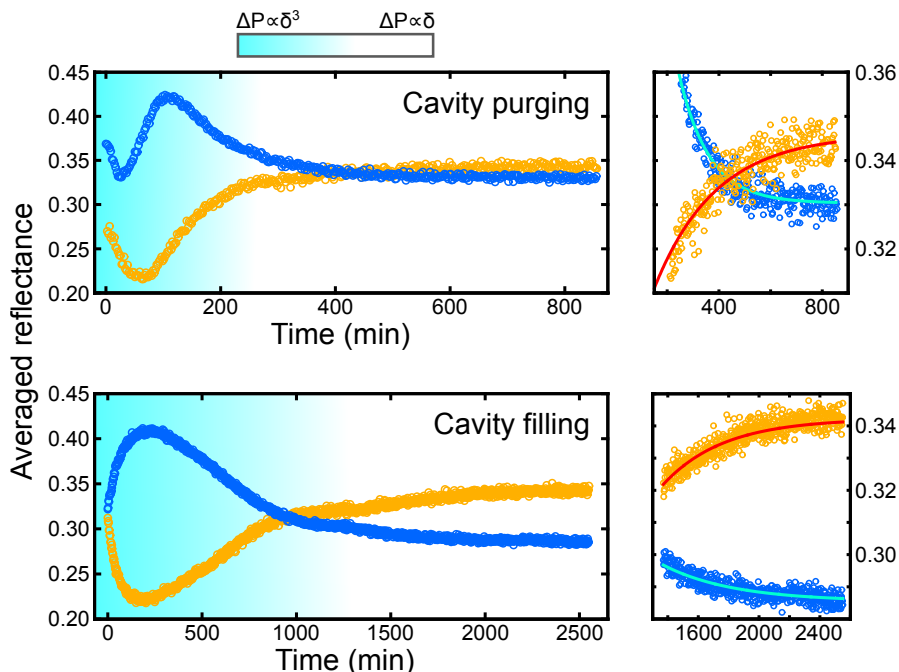

Figure 4: Change of drum averaged reflectance with time during purging and filling: time constant extraction. A simple exponential function is fitted to the linear-deflection regime of the drum averaged reflectance (blue circles for λ=460 nm and orange circles for λ=600 nm) to obtain the time constants of the drum when purging and filling (values showed in Table 1). The extracted time constants lead to a membrane permeance of around $1 \times 10^{-14} \frac{mol}{m^2 s \cdot Pa}$.

Air diffusion could be taking place through the graphene material, although we cannot discard the interface and oxide as diffusion channels. Further studies must be done to determine the actual diffusion channel/s on these systems. The permeance for the DLG membrane is calculated to be $(0.71 \pm 0.10)10^{-14} \frac{mol}{m^2 s \cdot Pa}$ from the filling data, and $(1.43 \pm$

8

Table 1: Values of time constants and permeances.

Wavelength (nm)	Filling		Purging	
	τ (min)	$\mathcal{P}$ ($10^{-14}\frac{mol}{m^2 s \cdot Pa}$)	τ (min)	$\mathcal{P}$ ($10^{-14}\frac{mol}{m^2 s \cdot Pa}$)
460	446	0.87	125	3.12
532	653	0.60	125	3.12
600	519	0.75	237	1.65
633	573	0.68	6294	0.06
660	570	0.69	565	0.69
AFM	1914	0.20	630	0.62

1.39)$10^{-14}\frac{mol}{m^2 s \cdot Pa}$ from the purging data, which are two to three orders of magnitude higher than the permeance measured in pristine BLG.[37] The spread in permeance values in Table 1 is larger in the purging experiment than in the filling case due to illumination difficulties that happen during the purging experiment and inaccuracies in the exponential fitting that can be large for certain wavelengths. Measurements performed by AFM yield similar permeance values and they unexpectedly show different values between filling and purging even in the small deflection regime (see Supporting Information). This discrepancy between purging and filling at small deflections is an indication that extra diffusion channels such as the graphene-oxide interface play a role in gas permeation.

The difference between purging and filling the cavity arising from the difference of molecular flux at large deflections is reproducible, which bring us to the conclusion that the change in volume of these ultrathin microdrums cannot be ignored. The effect becomes strong when the membranes are deflected beyond the linear regime, which is usually the case when performing AFM nanoindentation or pressure studies. To extend these conclusions to other drums and study the dependence with their diameter, we can apply the colorimetry technique to hundreds of drums (see Supporting Information).

This study has presented the colorimetry technique as a scalable tool to characterize the mechanical properties and the permeance of suspended graphene microdevices. This non-invasive optical technique allows to extract the evolution of a thin membrane deflection with time when filling and emptying the microcavity with air. We observe the linear-

and nonlinear-deflection regimes, and we find that the gas filling process is slower than the gas purging in the case of large deflection, where volume change is not negligible. Furthermore, we use small deflection measurements to extract the permeance of a double-layer CVD graphene membrane, finding that it is about two to three orders of magnitude higher than pristine BLG. Ultimately, the colorimetry technique could be employed to characterize the mechanical properties of suspended SLG and other 2D materials by using the right combination of cavity depth and wavelength. The parallelization of data acquisition by image processing tools combined with a controlled deformation of the membranes would allow the fast characterization of large arrays of these mechanical systems at once limited only by the resolution of the optical instrument, and could lead to the realization of interferometric modulator displays (IMOD) made out of graphene.

Acknowledgement

Supporting Information Available

Description of the CVD-SLG growth and CVD-DLG transfer. Gamma factor characterization and correction. Calculation of the geometric volume factor. Newton's rings fitting. Derivation of the drum averaged reflectance for small deflections. Drum averaged reflectance with time for all the wavelengths for gas purging and filling. Modeling the behavior of cavity purging and filling for large deflections. AFM measurement of the deflection as a function of time for gas purging and filling. Video of the change in color of the drum in a filling experiment. Animated extraction of the reflectance profile as a function of time for a wavelength (660 nm) when filling. Video of the change in color of hundreds of drums in a filling experiment.

This material is available free of charge via the Internet at `http://pubs.acs.org/`.

References

(1) Novoselov, K. S.; Geim, A. K.; Morozov, S. V.; Jiang, D.; Zhang, Y.; Dubonos, S. V.; Grigorieva, I. V.; Firsov, A. A. *Science* **2004**, *306*, 666–9.

(2) Zhang, Y. B.; Tan, Y. W.; Stormer, H. L.; Kim, P. *Nature* **2005**, *438*, 201–204.

(3) Koppens, F. H. L.; Chang, D. E.; García de Abajo, F. J.; Abajo, F. J. G. D. *Nano. Lett.* **2011**, *11*, 3370–3377.

(4) Bunch, J. S.; Verbridge, S. S.; Alden, J. S.; Van Der Zande, A. M.; Parpia, J. M.; Craighead, H. G.; McEuen, P. L. *Nano Letters* **2008**, *8*, 2458–2462.

(5) Yang, H.; Heo, J.; Park, S.; Song, H. J.; Seo, D. H.; Byun, K.-E.; Kim, P.; Yoo, I.; Chung, H.-J.; Kim, K. *Science* **2012**, *336*, 1140–3.

(6) Nair, R. R.; Wu, H. A.; Jayaram, P. N.; Grigorieva, I. V.; Geim, A. K. *Science* **2012**, *335*, 442–444.

(7) Smith, A. D.; Niklaus, F.; Paussa, A.; Vaziri, S.; Fischer, A. C.; Sterner, M.; Forsberg, F.; Delin, A.; Esseni, D.; Palestri, P.; Östling, M.; Lemme, M. C. *Nano Letters* **2013**, *13*, 3237–3242.

(8) Dolleman, R. J.; Davidovikj, D.; Cartamil-Bueno, S. J.; Van Der Zant, H. S. J.; Steeneken, P. G. *Nano Letters* **2016**, *16*, 568–571.

(9) Du, X.; Skachko, I.; Andrei, E. Y.; Barker, A. *Nature nanotechnology* **2008**, *3*, 491–5.

(10) Bolotin, K. I.; Sikes, K. J.; Jiang, Z.; Klima, M.; Fudenberg, G.; Hone, J.; Kim, P.; Stormer, H. L. *Solid State Communications* **2008**, *146*, 351–355.

(11) Bolotin, K. I.; Sikes, K. J.; Hone, J.; Stormer, H. L.; Kim, P. *Physical Review Letters* **2008**, *101*, 096802.

(12) Rickhaus, P.; Makk, P.; Liu, M.-H.; Tóvári, E.; Weiss, M.; Maurand, R.; Richter, K.; Schönenberger, C. *Nature communications* **2015**, *6*, 6470.

(13) Kim, Y. D. et al. *Nature Nanotechnology* **2015**, *10*, 1–7.

(14) Ferrari, A. C. et al. *Nanoscale* **2014**, *7*, 4598–4810.

(15) Suk, J. W.; Kitt, A.; Magnuson, C. W.; Hao, Y.; Ahmed, S.; An, J.; Swan, A. K.; Goldberg, B. B.; Ruoff, R. S. *ACS Nano* **2011**, *5*, 6916–6924.

(16) López-Polín, G.; Gómez-Herrero, J.; Gómez-Navarro, C. *Nano Letters* **2015**, *15*, 2050–2054.

(17) Frank, I. W.; Tanenbaum, D. M.; van der Zande, A. M.; McEuen, P. L. *Journal of Vacuum Science & Technology B: Microelectronics and Nanometer Structures* **2007**, *25*, 2558–2561.

(18) Meyer, J. C.; Geim, A. K.; Katsnelson, M. I.; Novoselov, K. S.; Booth, T. J.; Roth, S. *Nature* **2007**, *446*, 60–3.

(19) Bunch, J. S.; van der Zande, A. M.; Verbridge, S. S.; Frank, I. W.; Tanenbaum, D. M.; Parpia, J. M.; Craighead, H. G.; McEuen, P. L. *Science (New York, N.Y.)* **2007**, *315*, 490–493.

(20) Poot, M.; van der Zant, H. S. J. *Applied Physics Letters* **2008**, *92*, 063111.

(21) Lee, C.; Wei, X.; Kysar, J. W.; Hone, J.; =, *Science* **2008**, *321*, 385–388.

(22) Zande, A. M. V. D.; Barton, R. A.; Alden, J. S.; Ruiz-Vargas, C. S.; Whitney, W. S.; Pham, P. H. Q.; Park, J.; Parpia, J. M.; Craighead, H. G.; McEuen, P. L. *Nano letters* **2010**, *10*, 4869–4873.

(23) Barton, R. A.; Ilic, B.; van der Zande, A. M.; Whitney, W. S.; McEuen, P. L.; Parpia, J. M.; Craighead, H. G. *Nano letters* **2011**, *11*, 1232–6.

(24) Metten, D.; Federspiel, F.; Romeo, M.; Berciaud, S. *Physical Review Applied* **2014**, *2*, 1–11.

(25) Shin, Y.; Lozada-Hidalgo, M.; Sambricio, J. L.; Grigorieva, I. V.; Geim, A. K.; Casiraghi, C. *Applied Physics Letters* **2016**, *108*, 221907.

(26) Lee, G.-H.; Cooper, R. C.; An, S. J.; Lee, S.; van der Zande, A.; Petrone, N.; Hammerberg, A. G.; Lee, C.; Crawford, B.; Oliver, W.; Kysar, J. W.; Hone, J. *Science* **2013**, *340*, 1073–6.

(27) Hwangbo, Y.; Lee, C.-K.; Kim, S.-M.; Kim, J.-H.; Kim, K.-S.; Jang, B.; Lee, H.-J.; Lee, S.-K.; Kim, S.-S.; Ahn, J.-H.; Lee, S.-M. *Scientific reports* **2014**, *4*, 4439.

(28) O'Hern, S. C.; Stewart, C. A.; Boutilier, M. S. H.; Idrobo, J. C.; Bhaviripudi, S.; Das, S. K.; Kong, J.; Laoui, T.; Atieh, M.; Karnik, R. *ACS Nano* **2012**, *6*, 10130–10138.

(29) Celebi, K.; Buchheim, J.; Wyss, R. M.; Droudian, A.; Gasser, P.; Shorubalko, I.; Kye, J.-I.; Lee, C.; Park, H. G. *Science* **2014**, *344*, 289–292.

(30) Jessop, H. *Philosophical Magazine Series 6* **1921**, *42*, 551–568.

(31) Reserbat-Plantey, A.; Marty, L.; Arcizet, O.; Bendiab, N.; Bouchiat, V. *Nature nanotechnology* **2012**, *7*, 151–5.

(32) Ochoa-Martínez, E.; Gabás, M.; Barrutia, L.; Pesquera, A.; Centeno, A.; Palanco, S.; Zurutuza, A.; Algora, C. *Nanoscale* **2015**, *7*, 1491–1500.

(33) Georgiou, T.; Britnell, L.; Blake, P.; Gorbachev, R. V.; Gholinia, A.; Geim, A. K.; Casiraghi, C.; Novoselov, K. S. *Applied Physics Letters* **2011**, *99*, 2011–2013.

(34) Blake, P.; Hill, E. *Applied Physics Letters* **2007**, *063124*, 3.

(35) Renshaw, D.; Wang, G.; Denyer, P. B.; Lu, M. CMOS video cameras. Euro ASIC '91. 1991; pp 100–103.

(36) Young, W. C.; Budynas, R. G. *Library*; 2002; Vol. 7; p 832.

(37) Koenig, S. P.; Wang, L.; Pellegrino, J.; Bunch, J. S. *Nature nanotechnology* **2012**, *7*, 728–32.

(38) Koenig, S. P.; Boddeti, N. G.; Dunn, M. L.; Bunch, J. S. *Nature nanotechnology* **2011**, *6*, 543–6.

(39) *ASTM International* **2015**, *Designation D1434-82*, 1–13.

(40) Liu, X.; Suk, J. W.; Boddeti, N. G.; Cantley, L.; Wang, L.; Gray, J. M.; Hall, H. J.; Bright, V. M.; Rogers, C. T.; Dunn, M. L.; Ruoff, R. S.; Bunch, J. S. *Advanced Materials* **2014**, *26*, 1571–1576.

Supporting Information

Supporting Information Outline:

1. Description of the CVD-SLG growth and CVD-DLG transfer.

Single-layer graphene was grown by chemical vapour deposition (CVD) using a 4" cold wall reactor (Aixtron BM). Copper foil was used as the catalyst and a surface pre-treatment was carried out in order to remove the native copper oxide and other impurities. The synthesis was carried out at 1000°C using methane as the carbon source. After the synthesis, the single-layer graphene was coated with a polymer layer and stacked onto a second single-layer graphene by using a semi-dry transfer process. The stacked double-layer CVD graphene was transferred onto 5×5 mm^2 SiO$_2$/Si substrates containing circular cavities of 1-20 μm in size and 600 nm in depth by following a semi-dry transfer procedure. Finally, the supporting polymer layer was removed by annealing at 450°C for 2 hours in N$_2$ atmosphere.

2. Gamma factor characterization and correction.

Consumer CMOS cameras apply an artificial compression to the received intensity values. To characterize the gamma factor, we measured the intensity values reflected from the SiO$_2$ substrate for different illumination intensities by using neutral density filters. Figure S-1

shows the power relation of the curves for three wavelengths. We obtain an average gamma of 0.4545 for all the wavelengths.
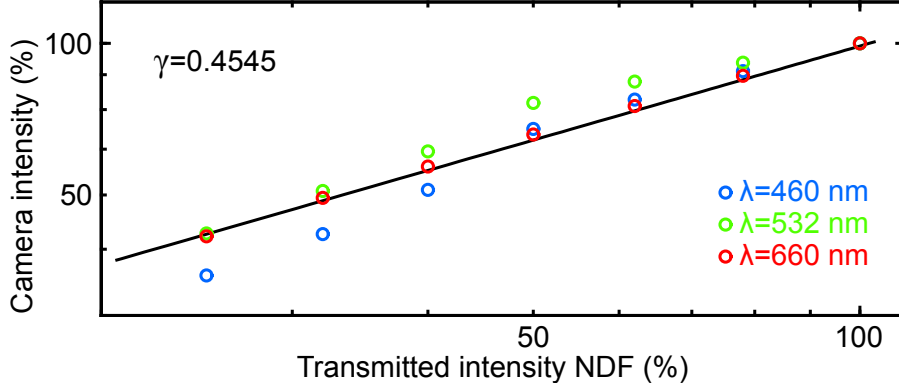

Figure S-1: Gamma characterization.

In the main text, we compensate for the compression by applying a gamma correction

$$I = 255 \left(\frac{I_{RAW}}{255} \right)^{2.2}.$$ (S-1)

3. Calculation of the geometric volume factor.

The volume of a membrane with a radial profile described by the membrane function $f(r) = 1 - 0.9\frac{r^2}{R^2} - 0.1\frac{r^5}{R^5}$ is obtained by integration. Thus,

$$
\begin{aligned}
V &= \delta_c \int_0^{2\pi} \int_0^R \left(1 - 0.9\frac{r^2}{R^2} - 0.1\frac{r^5}{R^5} \right) r \mathrm{d}r \mathrm{d}\theta \\
&= \pi R^2 \, 0.52 \, \delta_c.
\end{aligned}
$$ (S-2)

Therefore, $V = A\,b\,\delta_c$, where $A = \pi R^2$ and $b = 0.52$.

4. Newton's rings fitting.

Figure S-3 shows the Newton's rings reflectance data fitted to Eq. 1 for different deflections for both purging the air and filling the cavity (λ=532 nm). The Newton's rings fitting is used

16

in the main text to study the change in pressure-induced deflection with time, and therefore measure the permeance of the drum (Figure 3).
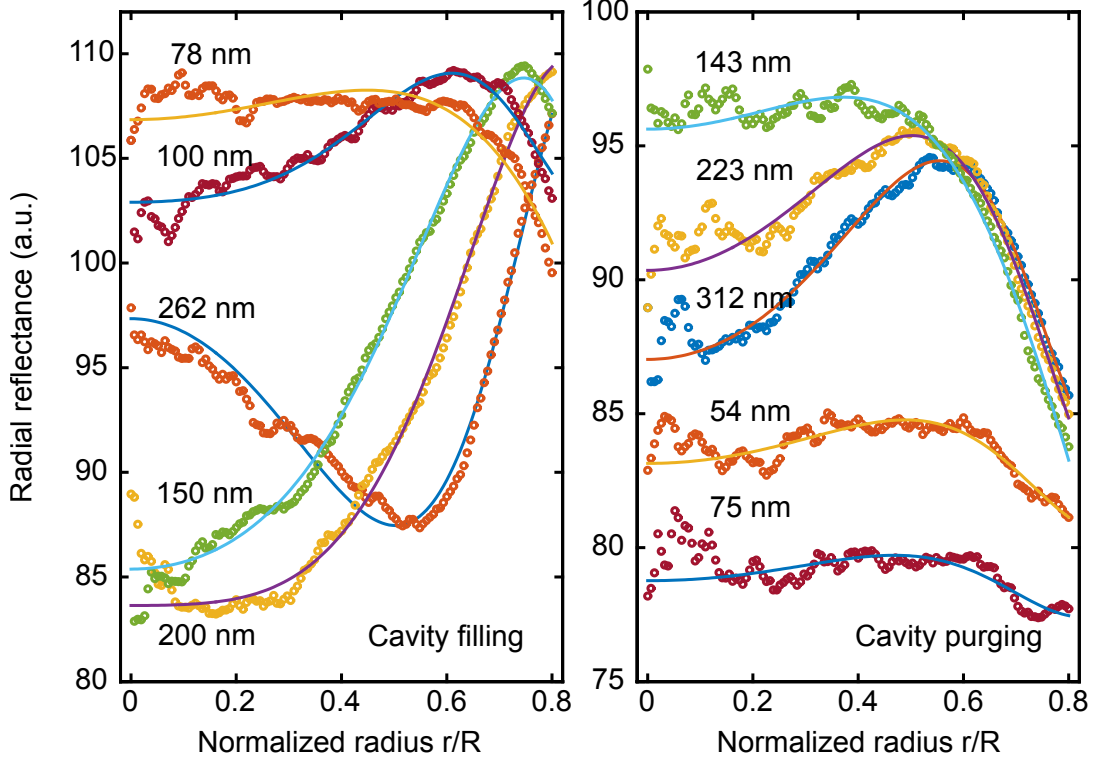

Figure S-2: Newton's rings fitting for different deflections.

5. Derivation of the drum averaged reflectance for small deflections.

The radial reflectance is

$$\mathcal{R}(r,t) \approx R_s + R_g + 2\sqrt{R_g R_s} \cos\left(\frac{4\pi}{\lambda}\left(g_0 - \delta(r,t)\right) + \phi\right) = R_s + R_g + 2\sqrt{R_g R_s}\cos(\Omega(t)\,f(r) + \phi'), \tag{S-3}$$

where $\Omega = -\frac{4\pi}{\lambda}\delta_c(t)$ and $\phi' = \frac{4\pi}{\lambda}g_0 + \phi$ are the spatial frequency and phase of a Newton ring. $f(r) = 1 - 0.9\frac{r^2}{R^2} - 0.1\frac{r^5}{R^5}$ is a profile function that can be approximated to $f(r) \approx 1 - \frac{r^2}{R^2}$ for small deflections. Then,

$$\mathcal{R}(r,t) \approx a + b\cos\left(-\frac{4\pi}{\lambda}\delta_c(t)\left(1 - \frac{r^2}{R^2}\right) + \phi'\right). \tag{S-4}$$

Taking the surface integral and using $rdr = \frac{R^2}{2}d\left(\frac{r^2}{R^2} - 1\right) = \frac{R^2}{2}dX$

$$\int_S \mathcal{R}(r,t)\,ds = \int_0^{2\pi}\int_0^R \mathcal{R}(r,t)\,rdrd\theta$$
$$\approx 2\pi \int_0^R \left[a + b\cos\left(\frac{4\pi}{\lambda}\delta_c(t)\left(\frac{r^2}{R^2} - 1\right) + \phi'\right)\right] rdr \tag{S-5}$$
$$\approx \pi R^2 a + \pi R^2 b \int_{-1}^0 \cos\left(\frac{4\pi}{\lambda}\delta_c(t)\,X + \phi'\right) dX$$
$$\approx \pi R^2 a + \pi R^2 b \frac{\lambda}{4\pi\delta_c(t)}\left[\sin(\phi') - \sin\left(\phi' - \frac{4\pi}{\lambda}\delta_c(t)\right)\right].$$

We can expand the second sine

$$\sin\left(\phi' - \frac{4\pi}{\lambda}\delta_c(t)\right) \approx \sin(\phi') - \frac{4\pi}{\lambda}\delta_c(t)\cos(\phi') - \frac{1}{2}\frac{4\pi}{\lambda}^2\delta_c^2(t)\sin(\phi'). \tag{S-6}$$

Therefore,

$$\mathcal{R}_{drum}(t) = a + b\frac{\lambda}{4\pi\delta_c(t)}\left(\sin(\phi') - \sin(\phi' - \frac{4\pi}{\lambda}\delta_c(t))\right)$$
$$\approx a + b\frac{\lambda}{4\pi\delta_c(t)}\left(\frac{4\pi}{\lambda}\delta_c(t)\cos(\phi') + \frac{1}{2}\frac{4\pi}{\lambda}^2\delta_c^2(t)\sin(\phi')\right) \tag{S-7}$$
$$\approx a + b\cos(\phi') + \frac{2\pi b}{\lambda}\sin(\phi')\delta_c(t).$$

For small deflections, we know that the change of deflection with pressure is a decaying exponential $\delta_c(t) = \delta_0\,e^{-t/\tau}$. Then,

$$\mathcal{R}_{drum}(t) \approx A + B\,e^{-t/\tau}, \tag{S-8}$$

where $A = a + b\cos(\phi')$, $B = \frac{2\pi b}{\lambda}\sin(\phi')\delta_0$, and δ_0 is the initial deflection in the linear regime.

6. Drum averaged reflectance with time for all the wavelengths for gas purging and filling.

Figure S-3 shows the drum average reflectance data for all the wavelengths for the purging (top) and filling (bottom) cases. Figure 4 in the main text uses this data for two wavelengths (460 nm and 600 nm).
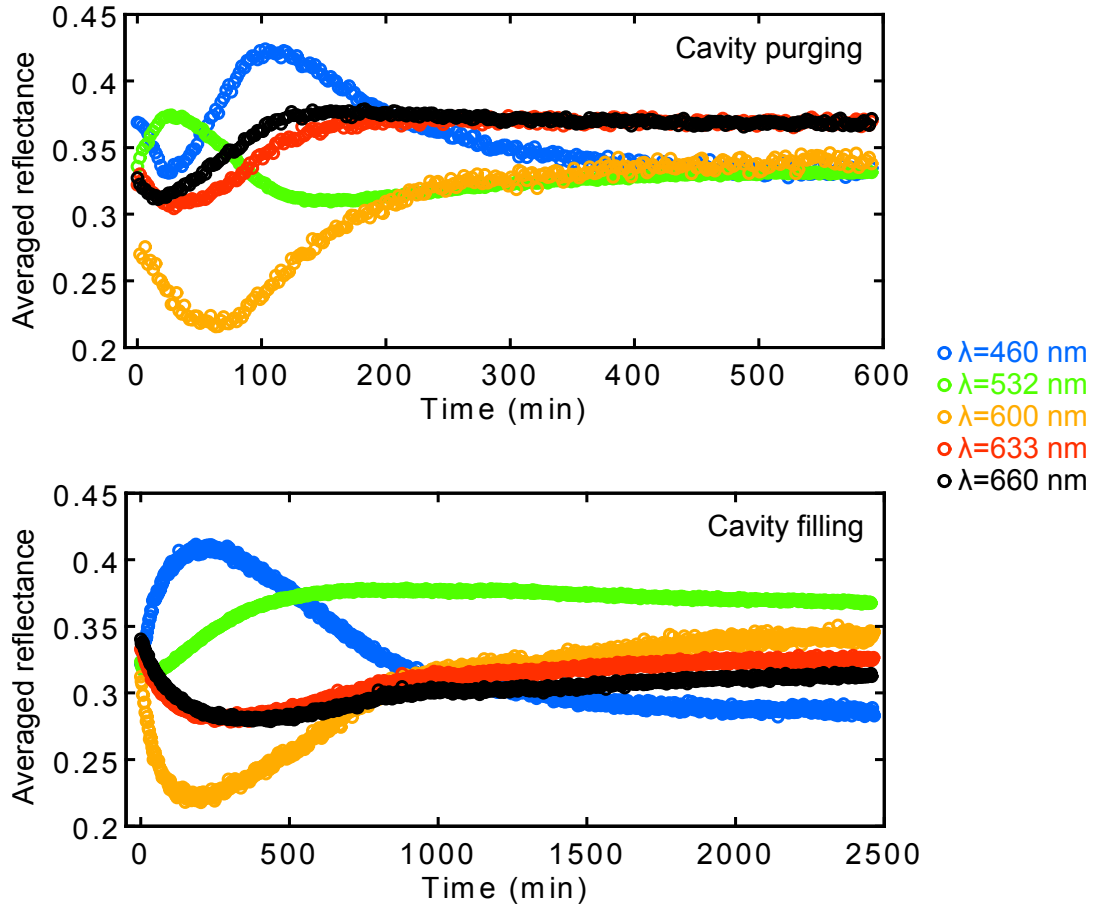

Figure S-3: Drum averaged reflectance for all wavelengths.

7. Modeling the behavior of cavity purging and filling for large deflections.

By applying Fick's law of diffusion $\frac{dn}{dt} = -\frac{\mathcal{P}}{A}\Delta P$ to Equation 2 in the main text, and given $\frac{\Delta P}{A} = k_3\delta^3$, we obtain:

$$\frac{d\delta}{dt} = \frac{\frac{-RT\mathcal{P}k_3}{A^2}}{4bk_3\delta^3 + 3g_0k_3\delta^2 + AbP_{ext}}. \tag{S-9}$$

Equation S-9 can be numerically integrated to obtain the time evolution of a deflating membrane. The curves below are plotted for purging and filling for the measured Young's modulus by AFM $E = 420$ GPa ($k_3 = 0.84\,10^{14}$ N/m^3) for different values of permeance.
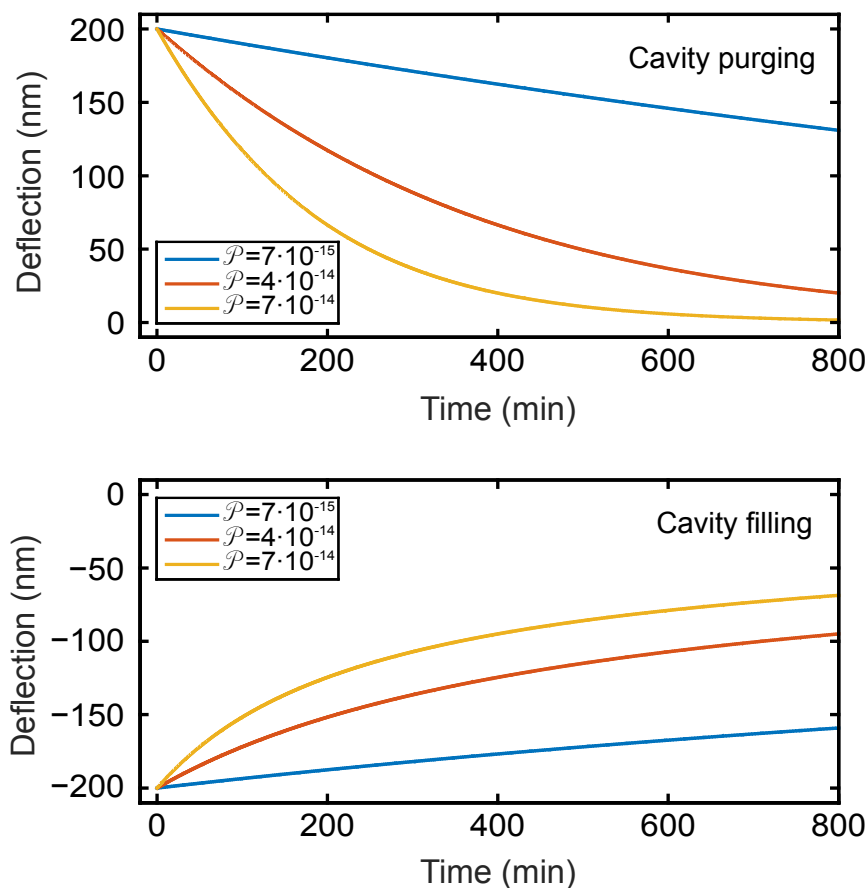

Figure S-4: Center deflection as a function of time for purging (top) and filling (bottom) experiments assuming a change of volume in the large deflection regime.

8. AFM measurement of the deflection as a function of time for gas purging and filling.

To compare the permeance values and the purging/venting difference, and validate the colorimetry technique we repeated the experiments to measure the deflection with a calibrated atomic force microscope (Bruker Fastscan, Scanassyst-Fluid tip). By using the Quantitative NanoMechanics mode (QNM) that allows a direct control of the maximum force applied to the substrate (Peak Force mode), we were able to image the height and extract the deformation of the suspended circular membrane of 13.2 μm in diameter at 5 nN. Figure S-6 shows the drum average deflection data for the purging (top) and filling (bottom) cases. Notice that the values of drum average deflection are a factor 0.52 from the actual deflection values at the center of the drum. Note that in the filling experiment we followed the same procedure as in the colorimetry technique (sample was left several days in a desiccator and moved to the AFM), while for the purging experiment we left the sample in an pressurized chamber at 2 bar for several days, hence having a positive pressure difference of 1 bar once returned to atmospheric pressure for AFM measurements.
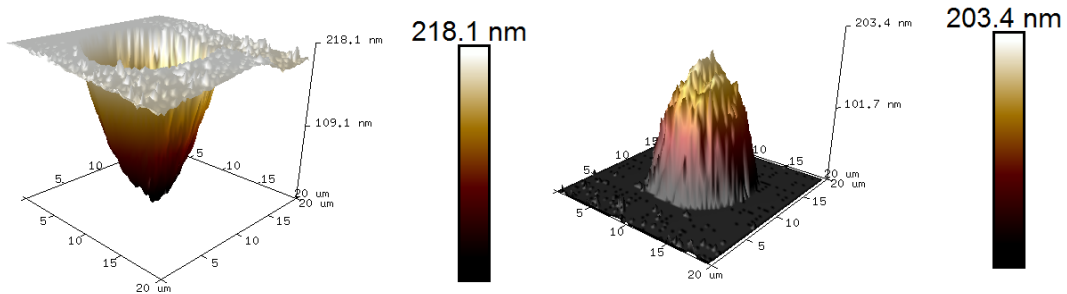

Figure S-5: 3D AFM height image of the drum at the beginning of the purging (left) and filling (right) experiments.

We also measured the roughness of the graphene-SiO_2 substrate in the surroundings of the drum. The R_a value obtained in an area free of wrinkles at the edge of the drum is
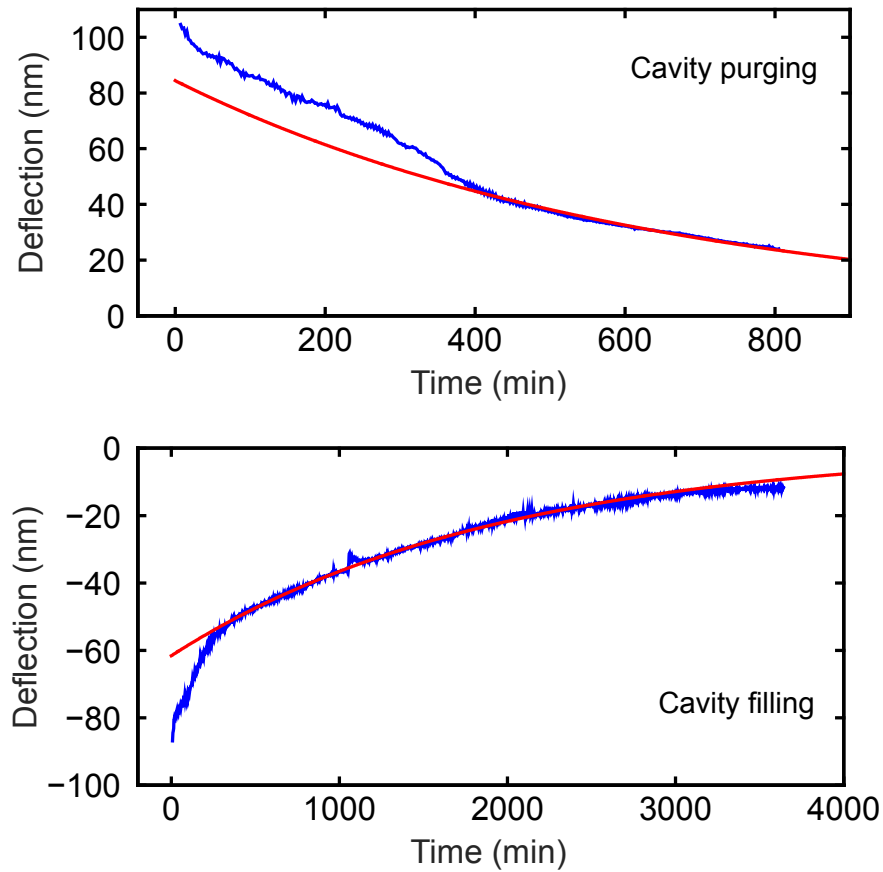
Figure S-6: Drum averaged deflection for purging (top) and filling (bottom) experiments.

0.3 nm, which is basically the roughness of the thermally-grown SiO_2. We also measured the roughness including wrinkles in the surroundings of the drum in question, and we read a R_a value of 2.2 nm. The gas permeation could happen through the interface, especially with the presence of wrinkles. However, we should not discard other diffusion channels such as the oxide and the material itself.

Graphical TOC Entry

$P_{ext}-P_{int} \approx 1$ bar $P_{ext}=P_{int}$

10 µm   10 µm